Electronic Basis of the Comparable Hydrogen Bond Properties of Small $H_2CO/(H_2O)_n$ and $H_2NO/(H_2O)_n$ Systems ($n = 1, 2$)

C. Houriez,[†] N. Ferré,*[,†] J.-P. Flament,[‡] M. Masella,[§] and D. Siri[†]

UMR CNRS 6517 "Chimie, Biologie, Radicaux Libres", Université de Provence, Faculté de Saint-Jérôme, Case 521, Avenue Escadrille Normandie-Niemen, 13397 Marseille Cedex 20, France, UMR CNRS 8523, Laboratoire de Physique des Lasers, Atomes et Molécules, Université de Lille 1, Bâtiment P5, 59655 Villeneuve d'Ascq, France, and Laboratoire de Chimie du Vivant, Service d'Ingénierie Moléculaire des Protéines, Institut de Biologie et de Technologies de Saclay, Commissariat à l'Energie Atomique, Centre de Saclay, 91191 Gif-Sur-Yvette Cedex, France

Received: July 2, 2007; In Final Form: August 28, 2007

The electronic and structural properties of dihydronitroxide/water clusters are investigated and compared to the properties of formaldehyde/water clusters. Exploring the stationary points of their potential energy surfaces (structurally, vibrationally, and energetically) and characterizing their hydrogen bonds (by both atoms in molecules and natural bond orbitals methods) clearly reveal the strong similarity between these two kind of molecular systems. The main difference involves the nature of the hydrogen bond taking place between the X−H bond and the oxygen atom of a water molecule. All the properties of the hydrogen bonds occurring in both kind of clusters can be easily interpreted in terms of competition between intermolecular and intramolecular hyperconjugative interactions.

1. Introduction

Nitroxides are spin-doublet radicals, whose single electron is mainly described by the π^* orbital of the N−O bond. They exhibit rather long half-life times and their electron paramagnetic resonance (EPR) spectra are highly sensitive to molecular mobility and environment.[1] That explains why they are widely used as spin probes to investigate the properties of biopolymers and nanostructures,[2] as well as controlling species in the living radical polymerization.[3] Moreover, nitroxides can be produced by the attachment of a transient free radical to a nitrone. In that case, the EPR spectrum of the resulting nitroxide is characteristic of both the nitroxide and the free radical. Such a procedure, referred to as "spin-trapping", is commonly used for monitoring reactions involving reactive radicals at concentrations too low for direct observations (such as the active forms of oxygen[4]). As in nearly every field of chemistry, hydrogen-bonding plays also a key role in the understanding of the EPR characteristics of the spin probe in solution. For instance, Barone and co-workers, who have shown a long standing interest for the computations of organics EPR spectra in condensed phase (cf., e.g., their recent review[5]), demonstrated the necessity of accounting explicitly for the interactions of the free radicals with the solvent molecules to compute accurate hyperfine coupling constants.

By contrast with the massive amount of experimental and theoretical results regarding hydrogen bonding among water molecules (whose current knowledge is still far from being complete[6]), only a few theoretical results are available concerning the interactions between nitroxides and water (see ref 5 and references therein): they all concern some particular structures, which cannot be used as such to draw a clear picture of these interactions. In particular, most of the theoretical studies devoted to nitroxide/water aggregates have focused on their global minimum and essentially ignored the rest of their potential energy surface (PES). However, it has been shown that the understanding of high-resolution experiments concerning small water aggregates (ranging from the dimer to the hexamers) needs to consider the rearrangement pathways connecting their global minimum.[7] Hence, reliable theoretical investigations of hydrogen-bonded systems have to focus not only on structures corresponding to minima but also on important stationary points of their PES.

Hence, the primary, but not sole, goal of this work is to theoretically investigate at different levels of theory the properties of several structures of the H_2NO/H_2O dimer and of the $H_2NO/(H_2O)_2$ trimer, corresponding to either minima or saddle points. This will provide further insight into hydrogen bonding involving nitroxides. Moreover, nitroxides can be seen as carbonyl compounds with an extra electron in a π^* orbital. That suggests that the properties of hydrogen bonds involving either a NO or a CO moiety are expected to be similar. To test this hypothesis, we have also investigated at the same levels of theory all the corresponding formaldehyde/water structures drawn by substituting H_2NO by H_2CO. To draw reliable conclusions, several properties have been considered, such as interaction energies, vibrational spectra, geometrical parameters as well as topological properties of the electronic density along the hydrogen bond axes. Particular attention was also devoted to evaluate the energetic incidence of cooperative effects on the heterotrimers, which are known to strongly affect the properties of hydrogen-bonded clusters by enhancing their hydrogen bond network.

Anticipating the results, we show that carbonyl/ and nitroxide/water clusters mainly differ by the hydrogen bond taking place between the X−H bond of the H_2XO moiety (X = C, N) and the water oxygen atom, whereas the properties of all the

* To whom correspondence should be addressed.
[†] Université de Provence.
[‡] Université de Lille 1.
[§] Institut de Biologie et de Technologies de Saclay.

10.1021/jp075136z CCC: $37.00 © 2007 American Chemical Society
Published on Web 10/18/2007

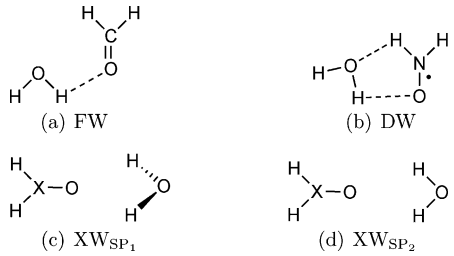

Figure 1. H_2XO/H_2O heterodimer: minimum and saddle points of the potential energy surface.

remaining hydrogen bonds are close. The electronic basis of these similarities (and differences) are mainly discussed in the present paper by considering the theoretical framework proposed by Weinhold and co-workers since 1988.[8] According to the latter authors, the properties of a hydrogen bond XH···Y mainly result from hyperconjugative interactions between the lone pairs of Y and the acceptor antibonding X−H orbitals.[9]

Note that the latter framework usually does not permit a simple interpretation of the so-called "blue-shifting hydrogen bonds", for which no fundamental difference compared to classical red-shifting ones has been evidenced (cf. ref 10 and the references mentioned therein). In 2003, in an attempt to propose an unified theoretical framework allowing for the explanation of the properties of both red- and blue-shifting hydrogen bonds, Weinhold and co-workers[11] proposed that the properties of a hydrogen bond XH···Y are the results of a subtle balance of the above hyperconjugative interactions and of rehybridization/repolarization phenomena affecting the properties of the X−H bond once the hydrogen bond is formed. Recently, Joseph and Jemmis[10] concluded that the latter approach is not able to explain all the known examples of blue-shifting hydrogen bonds, and they propose a simpler explanation: all hydrogen bonds face opposite contracting and lengthening forces. The first are due to the electron affinity of X, whereas the second are due to the attractive interaction between the positively charged proton H and the electron rich Y.

In the present report, we show that almost all the properties of the hydrogen bonds (whatever they correspond to red- or blue-shifting ones) occurring in the heteromers under investigation can be easily interpreted as arising from a competition between intra- and intermolecular hyperconjugative interactions. Hence, such a phenomenon represents also an important factor in understanding the fundamental properties of hydrogen bonds, as recently demonstrated by Li[12] and Liu and co-workers.[13]

2. Computational Details

2.1. Structures. All studied clusters are heterodimers or heterotrimers, composed by either a dihydronitroxide H_2NO (denoted by D hereafter) or a formaldehyde H_2CO (F) molecule interacting with one or two water molecules (W) (Figures 1 and 2).

As discussed below, the FW_{sp1} and DW_{sp1} nonplanar bifurcated C_{2v} dimer structures, as well as the FW_{sp2} and DW_{sp2} planar ones correspond to stationary points of the formaldehyde/water and dihydronitroxide/water PES. They have thus to be involved in the rearrangement processes of the FW and DW dimers by connecting their six equivalent global minima (obtained by interchanging the hydrogen atoms via rotations and tunneling). Their structures are comparable to those of the nonplanar and planar bifurcated C_{2v} structures of the water dimer, which have been recently investigated at high levels of theory.[14]

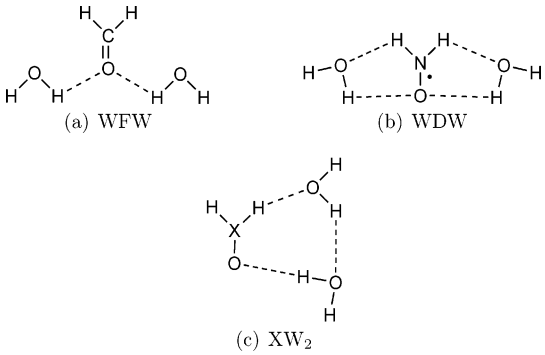

Figure 2. $H_2XO/(H_2O)_2$ heterotrimers: noncyclic and cyclic structures.

Among the structures considered here, the FW dimer and the FW_2 cyclic trimer have already been investigated at the MP2 level of theory:[15] they were shown to correspond to minima, and in the case of FW_2, strong stabilizing cooperative effects were shown to occur in it (they represent about 15% of the interaction energy). Moreover, a weak blue-shifting hydrogen bond CH−O_w was evidenced in the two aggregates. As far as we know, theoretical results concerning all the remaining complexes have never been reported.

Last, the water dimer (W_2) and the cyclic trimer (W_3) are also considered in the present study, for comparison purposes. Both have been intensively studied using high level ab initio computations and density functional methods, in conjunction with very extended basis sets.[14,16] As all cyclic hydrogen-bonded complexes, W_3 is strongly stabilized by cooperative effects (they represent about 15% of its interaction energy) and its hydrogen bonds are reinforced compared to that of W_2.

2.2. Theoretical Details. Standard ab initio and DFT computations were carried out by using the Gaussian 03 package of programs.[17] As an accurate description of hydrogen bonding requires flexible basis sets,[18,19,14] geometry optimizations were performed using the 6-311+G(d,p) basis set at three levels of theory: namely, the DFT (using the PBE0 and B3LYP functionals), the MP2, and the QCISD levels (with all electrons correlated).

The PBE0, B3LYP, and QCISD levels are commonly employed to investigate nitroxide radical properties, especially the spectromagnetic ones.[20,21,5,22] The PBE0, B3LYP, MP2, and QCISD levels were also shown to provide a proper description of hydrogen-bonded systems. In the particular case of the water dimer, the results reported at the MP2, PBE0, or B3LYP levels with intermediate size basis sets (such as 6-311+G(d,p) or aug-cc-pVTZ(-f)) are in good agreement with those derived from higher levels of theory, such as MP2-R12 and CCSD(T) with extended basis sets.[19,14]

The nature of the optimized structures was evaluated by computing their harmonic vibrational frequencies at the levels of theory mentioned above (however, only the dimer frequencies were computed at the QCISD level). Concerning the O−H stretching vibrational modes, the $\delta\nu_{O-H}$ shifts in the vibrational frequencies were computed by comparing the frequencies of the dimers and of the trimers to the $\bar{\nu}_{O-H}$ average frequency of the water monomer. In the case of X−H vibrational modes (X = C, N), an average shift $\delta\bar{\nu}_{X-H}$ is considered: it is computed by comparing the $\bar{\nu}_{X-H}$ average frequency value of the dimers and of the trimers to the values corresponding to the isolated F and D monomers.

As earlier studies exhibited,[23−25] quantum computations concerning hydrogen-bonded systems are affected by the basis set superposition error (BSSE), which can represent up to 10%

TABLE 1: B3LYP/6-311+G(d,p) Bond Distances (in Å), and Valence and Torsional Angles (in deg) of Water Dimer and Trimer (Average Values), Dihydronitroxide/Water and Formaldehyde/Water Clusters, X = C, N

	∠HXHO	r_{X-H}	r_{X-O}	$r_{XH\cdots O_w}$	r_{X-O_w}	$r_{OH_w\cdots O}$	r_{O_w-O}	$r_{OH_w\cdots O_w}$	$r_{O_w-O_w}$	∠XHO$_w$	∠OH$_w$O	∠OH$_w$O$_w$
W_2								1.932	2.900			174.8
W_3								1.904	2.783			148.5
F	179.9	1.108	1.202									
FW	180.0	1.105	1.207	2.816	3.222	1.992	2.874			101.4	150.1	
WFW	180.0	1.102	1.212	2.711	3.169	2.019	2.871			104.3	145.6	
				2.708	3.166		2.870				145.5	
FW_2	180.0	1.102 1.106	1.212	2.275	3.250	1.897	2.841	1.864	2.800	146.3	162.2	159.7
FW_{sp1}	180.0	1.107	1.203			2.636	3.127				112.0	
FW_{sp2}	180.0	1.107	1.204			2.540	3.028				111.5	
D	171.6	1.016	1.276									
DW	168.2	1.020 1.016	1.281	2.192	2.829	2.028	2.798			118.9	134.7	
WDW	179.9	1.019	1.284	2.190	2.832	2.039	2.801			119.3	133.9	
DW_2	177.2	1.029 1.016	1.283	1.895	2.874	1.838	2.786	1.816	2.740	157.8	161.7	155.9
DW_{sp1}	180.0	1.016	1.275			2.541	3.029				111.5	
DW_{sp2}	180.0	1.016	1.275			2.482	2.969				111.2	

of their interaction energies. In the present paper, the BSSE was estimated at the B3LYP/6-311+G(d,p) level using the full counterpoise method introduced by Boys and Bernardi.[26] For a system composed of *n* interacting molecules (*n*-mer), the BSSE is defined as

$$\mathrm{BSSE}_{n\text{-mer}} = \sum_{1}^{n}(E(\mathrm{mol})_{\mathrm{mol}} - E(\mathrm{mol})_{n\text{-mer}}) \qquad (1)$$

where $E(\mathrm{mol})_{\mathrm{mol}}$ represents the energy of a molecule calculated using its geometry within the *n*-mer and only its basis functions, and $E(\mathrm{mol})_{n-\mathrm{mer}}$ represents the energy of the same molecule using the full set of basis functions. To estimate the uncertainty of our calculations with respect to the basis set limit, single point energy computations were also performed at the B3LYP level using a more extended basis set (the 6-311+G(2df,2p)) on geometries optimized at the B3LYP/6-311+G(d,p) level.

To estimate the incidence of the cooperative effects on the trimers, the three-body interaction energies $\Delta E_{3-\mathrm{body}}$ were evaluated according to

$$\Delta E_{3\text{-body}} = \Delta E_{\mathrm{int}} - \sum \Delta E_{2\text{-body}} \qquad (2)$$

where ΔE_{int} corresponds to the total interaction energy of a trimer and $\Delta E_{2-\mathrm{body}}$ to the interaction energy of each dimer subunit.

To characterize the hydrogen bonds within the systems, the topological analysis of the electronic density ρ was performed using the Bader's AIM approach[27] implemented in the Gaussian 98 suite of programs.[28] When the properties of hydrogen-bonded systems are theoretically investigated, this analysis is commonly performed since it usually reveals the presence of a critical point (i.e., an extremum of the electronic density) along the axis of a hydrogen bond XH···Y. Typical values of the electronic density at the hydrogen bond critical point (ρ_C) range from 0.01 to 0.03 au, and a relationship exists between the magnitude of ρ_C and the hydrogen bond strength.[18,15]

The hyperconjugation interactions mentioned in Introduction are quantified in the present study by means of the NBO analysis, performed using the NBO v 3.15 program of the Gaussian 03 suite of programs. This analysis transforms a delocalized many-electron wavefunction into optimized electron pair bonding subunits, i.e., in a set of Lewis-type (such as σ bonding and lp lone pairs) and non-Lewis-type (such as Rydberg and σ^* antibonding) orbitals. The interactions among the latter two groups of orbitals can be used as a measure of the electronic delocalization within the systems under investigation. According to second-order perturbation theory arguments,[29] the strength of a hyperconjugative interaction between two orbitals γ_1 and γ_2 can be efficiently estimated from the magnitude of the charge q_c "transferred" between these two orbitals

$$q_c \approx \sum_{\alpha/\beta\ \mathrm{electrons}} \left(\frac{\langle\gamma_1|\hat{F}|\gamma_2\rangle}{\epsilon_{\gamma_1} - \epsilon_{\gamma_2}}\right)^2 \qquad (3)$$

Here, $\hat{F}$ is the Fock operator, and ϵ_{γ_1} and ϵ_{γ_2} are the energies of γ_1 and γ_2, in terms of diagonal Fock matrix elements. Other quantities can be used to quantify the hyperconjugation phenomena, like the bond-order descriptors arising in the natural resonance theory of Weinhold;[9] however, in the present paper, we have only considered the charge q_c.

3. Results and Discussion

3.1. Levels of Theory. A selected set of optimized geometrical parameters obtained at the B3LYP/6-311+G(d,p) level for the $H_2XO/(H_2O)_n$ systems (X = C, N) are listed in Table 1. The interaction energies ΔE_{int}, the vibrational frequencies ν_{X-H}, and the electronic density values at the bond critical point ρ_C for highlighted hydrogen bonds are summarized in Table 2. The results for the other levels of theory are available as Supporting Information.

Regardless of the level of theory, all of the heterotrimers and the DW and FW dimers correspond to minima. The DW_{sp1}, DW_{sp2}, and FW_{sp1} structures correspond to saddle points of their corresponding PES, whose order depends on the considered level of theory. All levels except MP2 predict DW_{sp1} to be a third-order saddle point, whereas DW_{sp2} is a transition state according to PBE0 and to MP2 and a second-order saddle point for B3LYP and for QCISD. Note that both B3LYP and QCISD predict a nonplanar structure for the D isolated monomer, whereas PBE0 and MP2 predict a planar one (cf. tables available as Supporting Information and discussion below). However, very small energy barriers (<1 kcal mol^{-1}) have been found at the B3LYP and QCISD levels concerning the inversion of the nitrogen center in the dihydronitroxide, meaning that the inversion is so easy that the mean experimental value should fall around 0°.

Regarding FW_{sp1}, it is predicted to be a third-order saddle point at the PBE0 and B3LYP levels and a second-order saddle point at the MP2 and QCISD levels. Last, FW_{sp2} is a transition state regardless of the level of theory.

To compare the different levels of theory, the results obtained at the DFT and MP2 levels are compared to those given by the highest level of theory employed, i.e., QCISD/6-311+G(d,p). To this end, the root-mean-square deviations (RMSD) concerning the geometries, the interaction energies for the minima, and

TABLE 2: B3LYP/6-311+G(d,p) Absolute Energies (in Hartrees), Interaction and 3-Body Energies (in kcal mol^{-1}), Number of Imaginary Frequencies, X−H Stretching Frequencies (in cm^{-1}), and Electronic Densities (in au) of Water Dimer and Trimer, Dihydronitroxide/Water, and Formaldehyde/Water Clusters, X = C, N

	E	ΔE_{int}	$\Delta E_{3\text{-body}}$	N	ν_{X-H}	$\rho_{C,XH\cdots O_w}$	$\rho_{C,OH_w\cdots O}$	$\rho_{C,OH_w\cdots O_w}$
W	−76.458 46			0				
W_2	−152.926 23	−5.842		0				0.0247
W_3	−229.402 95	−17.300	−2.836	0				0.0271
F	−114.541 76			0	2886			
					2944			
FW	−191.007 92	−4.832		0	2917		0.0223	
					2995			
WFW	−267.473 59	−9.356	−0.609	0	2947		0.0212	
					3038			
FW_2	−267.481 47	−14.301	−2.504	0	2915	0.0137	0.0275	0.0294
					3023			
FW_{sp1}	−191.004 28	−2.548		3				
FW_{sp2}	−191.005 01	−3.006		1				
D	−131.138 67			0	3425			
					3558			
DW	−207.608 81	−7.329		0	3403	0.0155	0.0224	
					3563			
WDW	−284.078 61	−14.445	−0.671	0	3396	0.0156	0.0219	
					3553			
DW_2	−284.087 19	−19.829	−4.009	0	3277	0.0286	0.0326	0.0333
					3540			
DW_{sp1}	−207.602 12	−3.131		3				
DW_{sp2}	−207.602 56	−3.407		2				

TABLE 3: Geometrical (in Å) and Energetic (in kcal mol^{-1}) RMSD from the QCISD Results (Using the 6-311+G(d,p) Basis Set)

		PBE0	B3LYP	MP2
$RMSD_G$	D	0.057	0.036	0.056
	DW	0.066	0.042	0.064
	DW_{sp1}	0.022	0.005	0.029
	DW_{sp2}	0.040	0.060	0.047
	WDW	0.058	0.035	0.063
	DW_2	0.067	0.047	0.052
$\langle RMSD_G \rangle$		0.052	0.038	0.052
$RMSD_E^{int}$		1.460	0.452	2.341
$RMSD_E^{sp}$		0.640	0.283	0.743
$RMSD_G$	F	0.004	0.003	0.002
	FW	0.036	0.056	0.056
	FW_{sp1}	0.010	0.013	0.008
	FW_{sp2}	0.026	0.010	0.003
	WFW	0.065	0.129	0.018
	FW_2	0.059	0.037	0.028
$\langle RMSD_G \rangle$		0.033	0.041	0.020
$RMSD_E^{int}$		0.748	0.384	0.499
$RMSD_E^{sp}$		0.457	0.277	0.274

the relative energies for the saddle points are computed for all systems (Table 3), according to

$$\mathrm{RMSD} = \sqrt{\frac{1}{N}\sum_{i=1}^{N}(x_i - x_{\mathrm{iref}})^2} \qquad (4)$$

Here, the reference corresponds to the QCISD results. For the geometrical RMSD ($RMSD_G$), N is the number of considered atoms and the sum runs over their Cartesian coordinates, whereas for the energetic RMSD ($RMSD_E$), N is the number of systems and x their interaction energies or relative energies.

Concerning the geometries, all levels provide results fairly close to the QCISD ones: regardless of the system and of the level of theory, the $RMSD_G$ values are at most 0.07, except for the WFW trimer at the B3LYP level, for which $RMSD_G$ reaches a value of 0.13. In the case of the nitroxide systems, the B3LYP $RMSD_G$ values correspond on average to the smallest (about 0.04). For the carbonyl systems, the MP2 level leads on average to results closer to the QCISD ones ($\langle RMSD_G \rangle = 0.02$), whereas

TABLE 4: Interaction Energy ΔE_{intI} and Basis Set Superposition Error BSSE at the B3LYP/6-311+G(d,p) Level and Interaction Energy ΔE_{intII} at the B3LYP/6-311+G(2df,2p)//B3LYP/6-311+G(d,p) Level (in kcal mol^{-1})

	ΔE_{intI}	$BSSE_I$	ΔE_{intII}
DW	−7.329	0.439	−6.802
WDW	−14.445	0.985	−13.266
DW_2	−19.829	1.688	−17.966
FW	−4.832	0.295	−4.487
WFW	−9.356	0.552	−8.591
FW_2	−14.301	1.180	−12.764

they are slightly larger for PBE0 and B3LYP (0.03 and 0.04, respectively). All levels predict a planar conformation for the formaldehyde in all clusters, as well as in the F isolated monomer, whereas the dihydronitroxide out-of-plane angle varies from 0 to 25° (and only the B3LYP values are consistent with the QCISD ones, cf. Supporting Information). This agreement between B3LYP and QCISD geometries has already been reported by Barone.[30] Note that he has also shown[31] that the large QCISD out-of-plane angle (25°) is reduced to 16.9° when the triple excitations are included in a perturbative manner.

On the other hand, the $RMSD_E$ values allow one to make a clear distinction among the levels. Considering first the interaction energies, $RMSD_E^{int}$ range from 0.45 to 2.34 kcal mol^{-1} for the nitroxide systems and from 0.38 to 0.75 kcal mol^{-1} for the carbonyl systems. Clearly, the B3LYP interaction energies are always the closest to the QCISD ones. Concerning the saddle point structures of the FW dimer, the MP2 level leads to the smallest $RMSD_E^{sp}$ value but the B3LYP value is marginally larger than this one (by only 0.003). Once again, the B3LYP $RMSD_E^{sp}$ value is the lowest for the nitroxide.

In summary, the B3LYP level provides satisfying and accurate results with respect to the QCISD ones for the geometrical and the energetic properties of both the dihydronitroxide/water and the formaldehyde/water systems. In the particular case of dihydronitroxide systems, the results agree with an earlier conclusion of Barone.[31] Concerning the BSSE, the results listed in Table 4 show that the BSSE values computed at the B3LYP/6-311+G(d,p) level do not exceed 8.5% of the system interaction energies: they are about 0.4 kcal mol^{-1} for

the dimers and they range from 0.6 to 1.7 kcal mol^{-1} for the trimers. The latter values are in good agreement with those reported in earlier studies of small hydrogen-bonded systems at the same level of theory with similar basis sets.[32,33] Interestingly, the difference between interaction energies computed, respectively, at the B3LYP/6-311+G(2df,2p)//B3LYP/6-311+G(d,p) and B3LYP/6-311+G(d,p) levels are of the same order of magnitude as the BSSE values computed at the B3LYP/6-311+G(d,p) level.

Hence, all the following discussions concerning the nitroxide and the carbonyl systems will be based on the B3LYP results.

3.2. Formaldhyde and Dihydronitroxide Systems. *3.2.1. Formaldehyde/Water $H_2CO/(H_2O)_n$ Systems.* Regarding the formaldehyde systems, the FW dimer and the FW_2 cylic trimer have been already investigated at the MP2 level of theory.[15] Compared to our B3LYP results, those earlier results differ at most by a few percentages for all of the properties discussed in the present paper (geometries, vibrational spectra, interaction energies, and electronic density at hydrogen bond critical points).

Regarding the FW dimer and as previously reported, our computations exhibit the existence of a classical red-shifting hydrogen bond $O_wH\cdots O$ and of a weak blue-shifting hydrogen bond $CH\cdots O_w$ (compared to the F monomer, the C−H bond length is shortened by 0.003 Å and the $\delta\bar{\nu}_{C-H}$ frequency is shifted to the blue by 41 cm^{-1}). The properties of the red-shifting hydrogen bond match those of classical hydrogen bonds: its length is 1.99 Å and its ρ_C value is 0.022 au at the B3LYP level. The main difference between this hydrogen bond and prototypical red-shifting ones, such as that occurring in the W_2 water dimer, concerns the $\angle O_wHO$ angle, which is predicted by all levels of theory to range between 146 and 150°. Such a distorted structure results from the presence of the $CH\cdots O_w$ interaction. However, (1) as no critical point along the $CH\cdots O_w$ axis is highlighted by the topological analysis of the electronic density and (2) as the $CH\cdots O_w$ distance is about 2.81 Å, this hydrogen bond is particularly weak.

Among the three dimer structures, only FW is a minimum and the FW_{sp1} and FW_{sp2} saddle points are higher in energy than FW by, respectively, 2.3 and 1.8 kcal mol^{-1}. FW_{sp1} and FW_{sp2} are close to the nonplanar and planar bifurcated C_{2v} structures of the water dimer, investigated first at the MP2 level by Smith and co-workers in 1990[34] and reinvestigated more recently at higher levels of theory (up to the CCSD(T) level) by Tschumper and co-workers[14] (in the latter study, the two structures are denoted by no. 9 and no. 10 and they correspond to a nonplanar transition state and to a planar higher-order saddle point, respectively). At the difference of the water dimer, the FW_{sp2} planar bifurcated structure is predicted by all theory levels to be a transition state, whereas the FW_{sp1} nonplanar bifurcated structure is predicted to be a higher-order saddle point (whose order, 2 or 3, depends on the level of theory). However, the difference in energy ΔE_{sp} between the no. 9 water dimer stationary point and the W_2 water dimer global minimum is equal to the difference in energy between the FW_{sp2} stationary point and the FW minimum: regardless of the level of theory, ΔE_{sp} range from 1.7 to 1.9 kcal mol^{-1} (Table 2 and refs 34,14). Similarly, the difference in energy ΔE_{sp} between FW_{sp1} and FW is also close to the difference in energy between no. 10 and W_2: they range between 2.3 and 2.7 kcal mol^{-1} (Table 2 and refs 34,14).

As may be seen in Table 2, the interaction energy of the WFW trimer is 2 times larger than the FW dimer one (respectively, −4.8 and −9.4 kcal mol^{-1}), and the cooperative effects are slightly stabilizing for this trimer: they account for 6.5% of its interaction energy. Both the trimer $OH_w\cdots O$ hydrogen bonds present very close properties with that observed in FW, with regard to the bond lengths (2.03 Å), to the $\angle OH_wO$ angle values (146−150°), and to the values of ρ_C (0.021 au). Similarly, most of the properties of the $CH\cdots O_w$ interactions in WFW are fully comparable to those of the $CH\cdots O_w$ hydrogen bond of FW: the $CH\cdots O_w$ distances are about 2.71 Å and no critical point is observed along the $CH\cdots O_w$ axis. However, it may be noticed that, compared to the values in the F monomer, the two C−H bonds are shortened by 0.006 Å and their $\bar{\nu}_{C-H}$ mean frequency is now blue-shifted by 78 cm^{-1}. Even if these values are about 2 times larger than in FW, their magnitudes are comparable in FW and WFW. Hence, each water molecule interacts with H_2CO in WFW in the same way as in FW, without being affected by the presence of the second water molecule. That may explain the weak incidence of cooperative effects on this symmetric trimer.

An additional hydrogen bond between the two water molecules is observed in the FW_2 cyclic trimer, compared to the WFW symmetric one. FW_2 is also more stable than WFW (its interaction energy is −14.3 kcal mol^{-1}), and the cooperative effects have a stronger incidence on it: they are stabilizing and they account for 17.5% of its interaction energy. As previously reported, this strong incidence of stabilizing cooperative effects is related to a global reinforcement of the hydrogen bond network within FW_2. For instance, the $OH_w\cdots O$ hydrogen bond is here shortened by about 0.1 Å and the electronic density at the critical point is larger by 20%, as compared to FW and WFW. The most remarkable interaction reinforcement in FW_2 concerns the $CH\cdots O_w$ interaction: the $CH\cdots O_w$ distance is significantly shortened compared to FW and WFW (by 0.4 and 0.5 Å, respectively), and a critical point is now observed along the $CH\cdots O_w$ axis with a density value of 0.014 au. However, for the $\bar{\nu}_{C-H}$ frequency, a weaker blue shift is observed in FW_2 than in WFW: they are, respectively, 54 and 78 cm^{-1}. Last, the properties of the hydrogen bond between the two water molecules of FW_2 are comparable to those of the hydrogen bonds occurring in the W_3 cyclic water trimer, which are also reinforced compared to that of W_2 (Table 2).

3.2.2. Dihydronitroxide/Water $H_2NO-(H_2O)_n$ Systems. Considering the results summarized in Table 2, the DW structure corresponds to a minimum. Its interaction energy is −7.3 kcal mol^{-1} and its out-of-plane angle is about 12°, which is close to the value observed in the isolated monomer (about 8°). As discussed in Section 3.1, the DW_{sp1} and DW_{sp2} geometries correspond to saddle points, whose order depends on the level of theory. Their interaction energies are greater than the DW one by about 4.2 and 3.9 kcal mol^{-1}, respectively.

The interaction energy of the WDW symmetric trimer is almost twice that of the DW dimer (−14.4 and −7.3 kcal mol^{-1}, respectively), while the DW_2 cyclic trimer is more stable than WDW by 5.4 kcal mol^{-1}. From the results presented in Table 2, the cooperative effects are stabilizing for the two trimers, however, they affect in a stronger manner the cyclic one: the cooperative contribution ΔE_{3-body} represents 20.2% of the DW_2 interaction energy and only 4.6% in the case of WDW.

The electronic density analysis evidences two types of hydrogen bonds in DW and WDW: the $NH\cdots O_w$ and $OH_w\cdots O$ bonds (Figures 1 and 2). The properties of each type of hydrogen bond are particularly close in both aggregates. For instance, the $NH\cdots O_w$ hydrogen bonds are characterized by ρ_C values of about 0.016 au, by hydrogen bond lengths of about 2.19 Å and by $\angle NHO_w$ angles of about 119°. Relative to the D isolated monomer, the NH groups involved in the latter hydrogen bonds

TABLE 5: Shifts of the X−H Distance (in Å) and of the X−H and O−H Stretching Frequencies (in cm^{-1}) with Respect to the Monomer Values, X = C, N

	Δr_{X-H}	$\Delta \nu_{X-H}$	$\Delta \nu_{O-H}$
DW	0.004	−9	−186
	0.000		
WDW	0.003	−17	−174
DW_2	0.013	−83	−381
	0.000		−320
FW	−0.003	41	−155
WFW	−0.006	78	−138
FW_2	−0.006	54	−237
	−0.002		−281

are characterized by a very weak increase of their bond length r_{N-H} (about $3\ 10^{-3}$ Å) and a small red shift in the $\bar{\nu}_{N-H}$ average frequency is observed in DW and WDW (respectively, −9 and −17 cm^{-1}, Table 5). Similarly, concerning the $OH_w\cdots O$ hydrogen bonds, their ρ_C values are about 0.022 au, their bond lengths $r_{OH_w}\cdots O$ about 2.03 Å, and their $\angle OH_wO$ angle values about 134−135° in DW and WDW. Hence, these results show that in WDW, each water molecule interacts with H_2NO in the same way as in DW, without being affected by the presence of the second water molecule. The results are related to the weak incidence of cooperative effects on the WDW symmetric trimer.

In the DW_2 cyclic heterotrimer, the topological analysis of the electronic density highlighted three hydrogen bonds: compared to WDW, there exists here an additional hydrogen bond between the two water molecules (Figure 2). From the results summarized in Tables 1 and 2, each of these hydrogen bonds is significantly reinforced in DW_2, as compared to the hydrogen bonds of W_2 and DW. For instance, in the trimer, and compared to the dimers, the r_{XH-O} hydrogen bond lengths are shorter by 0.1−0.3 Å and the values of ρ_C are reinforced by 30−100%. In the particular case of the $NH\cdots O_w$ hydrogen bond, and relative to the D isolated monomer, the N−H bond is elongated by 0.013 Å and a more pronounced red shift in the $\bar{\nu}_{N-H}$ average frequency is also observed (−83 cm^{-1}). These values are from 2−4 times larger than those obtained from the comparison between DW and D. Similarly, the hydrogen bond between the two water molecules of DW_2 is stronger than that occurring in the W_2 water dimer, and its properties are close to those of the W_3 cyclic water trimer (Tables 1 and 2). For instance, the DW_2 r_{OH-O_w} distance is 2.74 Å, whereas it is 2.90 Å in W_2 and 2.78 Å on average in W_3.

Clearly, the three hydrogen bonds of DW_2 are much stronger than those of the DW and W_2 dimers and, therefore, than those of the WDW symmetric trimer. These stronger hydrogen bonds are related to strong stabilizing cooperative effects occurring in DW_2, and all these results are characteristic of systems presenting a cyclic hydrogen bond pattern.

3.2.3. Comparison of Formaldehyde and Dihydronitroxide Systems. From the above results, the hydrogen bond network of both the formaldehyde and the dihydronitroxide systems present very close properties, in terms of geometry, of vibrational spectrum, and of electronic density. The main differences concern the interaction energies, which are systematically stronger for nitroxide systems, and the properties of the $X-H\cdots O_w$ hydrogen bonds, which correspond on average to blue-shifting ones in the case of H_2CO and to red-shifting ones in the case of H_2NO.

In particular, the PESs of the heterodimers present several similarities: their global minima correspond to a cyclic structure with two hydrogen bonds (O−H···O and $X-H\cdots O_w$), and the planar and nonplanar bifurcated C_{2v} structures shown in Figure 1 correspond to important stationary points of their respective PESs. As mentioned above, the three main differencies between the heterodimers concern the interaction energy, which is stronger by about 2 kcal mol^{-1} for DW than for FW, the position in energy of the $DW_{sp1,2}$ and the $FW_{sp1,2}$ extrema (which, respectively, lie 4 and 2 kcal mol^{-1} higher in energy than the DW and FW global minima), and last, the properties of the $X-H\cdots O_w$ hydrogen bond. In the particular case of DW, this bond can be defined as a weak red-shifting one, whereas for FW, it corresponds to a blue-shifting one (the respective average shifts are −9 and 41 cm^{-1}).

Concerning the WFW and WDW symmetric heterotrimers, their properties are comparable to those of the heterodimers. Note in particular that each of their water molecules interact with the H_2XO moiety in the same way as in the FW and DW dimers, without being affected by the presence of the second water molecule. This is supported by the weak incidence of cooperative effects in the two trimers: they account for about 5% of their interaction energies, which are twice those of the corresponding dimers within a few tenths of a kcal mol^{-1}. The main differences between the two symmetric heterotrimers match the differences observed between the heterodimers: the interaction energy is stronger by 5 kcal mol^{-1} for WDW than for WFW and their $X-H\cdots O_w$ hydrogen bonds correspond, respectively, to blue-shifting ones for WFW (with a mean shift of 78 cm^{-1}) and to weak red-shifting ones for WDW (with a mean shift of −17 cm^{-1}).

Finally, the hydrogen bond network of the DW_2 and FW_2 cyclic heterotrimers are also very close. It is made of three hydrogen bonds ($XH\cdots O_w$, $OH_w\cdots O$, and $OH_w\cdots O_w$), and as in all hydrogen-bonded trimers with a cyclic donor/acceptor pattern, strong cooperative effects occur in them (they account for 17−20% of their interaction energies). Regarding their remaining properties, they are all very close, except for the interaction energies (stronger by 5 kcal mol^{-1} for DW_2 than for FW_2) and the properties of their $X-H\cdots O_w$ hydrogen bond, which corresponds to a red-shifting one for DW_2 and to a blue-shifting one for FW_2. However, the average red shift is more pronounced for DW_2 than for WDW (respectively, −83 and −17 cm^{-1}), whereas the mean blue shift is less pronounced for FW_2 than for WFW (respectively, 54 and 78 cm^{-1}).

3.3. Electronic Basis of the Similarities between Formaldehyde and Dihydronitroxide Systems. *3.3.1. Intra- and Intermolecular Hyperconjugation Competition.* To understand the origin of the similarities (and differences) between the nitroxide and the formaldehyde systems, we may consider the NBO results listed in Tables 6 −8 (the atom numbering follows the convention given in Figure 3). These results concern the lp (O) → σ^* (X−H) and the lp (O) → σ^* (O−H) hyperconjugative interactions occurring in the systems, as well as the electronic population of the σ^* (X−H) antibonding orbitals shown in Figure 4. Notice that the values discussed in the following paragraphs reflect all of the NBO results, whereas Tables 6−8 only report significant values ($q_c \geq 0.001\ e$). The full NBO results are given in Supporting Information.

Concerning the F and D monomers (Table 6), the NBO analysis reveals the existence of two lone pairs located on their oxygen atom. One of these lone pairs corresponds to a sp orbital oriented along the X−O axis, whereas the second one corresponds to a pure p orbital orthogonal to this axis and to the π cloud of the X−O bond. A double intramolecular hyperconjugative interaction between the oxygen p lone pair and the two σ^* (X−H) antibonding orbitals exists in the two monomers; however, this interaction is stronger for F: the charge q_c "transferred" from the p lone pair toward each antibonding

TABLE 6: NBO Hyperconjugation Results (in Hartrees and *e*) for the Monomers and the Heterodimers (for $q_c \geq 10^{-3}$, cf. Supporting Information for the Complete Results)[a]

		$\Delta\epsilon$	$F(1, 2)$	q_c
F	LP2(O1)^p−BD*(C2H3)	0.62	0.106	0.0585
	LP2(O1)^p−BD*(C2H4)	0.62	0.106	0.0585
D	LP3(O1)^p−BD*(N2H3)	0.65	0.081	0.0328
		0.64	0.084	
	LP3(O1)^p−BD*(N2H4)	0.65	0.081	0.0328
		0.64	0.084	
FW	LP2(O1)^p−BD*(C2H3)	0.65	0.102	0.0492
	LP2(O1)^p−BD*(C2H4)	0.64	0.104	0.0528
	LP1(O1)−BD*(O5H6)	1.21	0.028	0.0011
	LP2(O1)^p−BD*(O5H6)	0.78	0.055	0.0099
DW	LP1(O1)−BD*(N2H3)	1.18	0.027	0.0012
		1.16	0.030	
	LP3(O1)^p−BD*(N2H3)	0.68	0.076	0.0260
		0.67	0.078	
	LP3(O1)^p−BD*(N2H4)	0.67	0.080	0.0297
		0.66	0.082	
	LP3(O1)^p−BD*(O5H6)	0.75	0.052	0.0103
		0.73	0.054	
	LP1(O5)−BD*(N2H3)	0.81	0.036	0.0039
		0.82	0.036	

[a]The p superscript indicates the strong p character of the corresponding orbital. For unrestricted calculations, both α and β contributions are given.

TABLE 7: NBO Hyperconjugation Results (in Hartrees and *e*) for the Symmetric Heterotrimers (for $q_c \geq 10^{-3}$, cf. Supporting Information for the Complete Results)[a]

		$\Delta\epsilon$	$F(1, 2)$	q_c
WFW	LP2(O1)^p−BD*(C2H3)	0.66	0.100	0.0459
	LP2(O1)^p−BD*(C2H4)	0.66	0.100	0.0459
	LP1(O1)−BD*(O5H6)	1.22	0.027	0.0010
	LP2(O1)^p−BD*(O5H6)	0.78	0.050	0.0082
	LP1(O1)−BD*(O8H9)	1.22	0.027	0.0010
	LP2(O1)^p−BD*(O8H9)	0.78	0.050	0.0082
WDW	LP3(O1)^p−BD*(N2H3)	0.69	0.076	0.0253
		0.68	0.078	
	LP3(O1)^p−BD*(N2H4)	0.69	0.076	0.0253
		0.68	0.078	
	LP3(O1)^p−BD*(O5H6)	0.76	0.050	0.0091
		0.74	0.051	
	LP3(O1)^p−BD*(O8H9)	0.76	0.050	0.0091
		0.74	0.051	
	LP2(O5)−BD*(N2H3)	0.81	0.038	0.0042
		0.82	0.037	
	LP2(O8)−BD*(N2H4)	0.81	0.038	0.0042
		0.82	0.037	

[a]The p superscript indicates the strong p character of the corresponding orbital. For unrestricted calculations, both α and β contributions are given.

orbital is 5.85×10^{-2} *e* for F and 3.28×10^{-2} *e* for D. Regardless of the monomers, the lp (O) → σ* (X−H) interactions are responsible for almost all the occupancy of the σ* (X−H) antibonding orbitals. Last, for D, the NBO analysis reveals also a weaker hyperconjugation between the oxygen sp lone pair and the two σ* (N−H) orbitals ($q_c = 0.08 \times 10^{-2}$ *e*), which are related to the nonplanar structure of D.

Concerning the FW and DW dimers (Table 6), the NBO analysis exhibits a weakening of the latter intramolecular hyperconjugative interactions. It also highlights the presence of a medium range hyperconjugation between the oxygen p lone pair of H_2XO and a water σ* (O−H) antibonding orbital, as well as a weaker hyperconjugation involving the H_2XO sp lone pair and the latter orbital. Hence, a part of the charge q_c transferred from the oxygen p lone pair toward the σ* (X−H) within F and D is now transferred toward a water σ* (O−H)

TABLE 8: NBO Hyperconjugation Results (in Hartrees and *e*) for the Cyclic Heterotrimers (for $q_c \geq 10^{-3}$, cf. Supporting Information for the Complete Results)[a]

		$\Delta\epsilon$	$F(1, 2)$	q_c
FW_2	LP1(O1)−BD*(C2H3)	1.10	0.026	0.0011
	LP2(O1)^p−BD*(C2H3)	0.68	0.096	0.0400
	LP2(O1)^p−BD*(C2H4)	0.64	0.103	0.0518
	LP1(O1)−BD*(O5H6)	1.19	0.045	0.0029
	LP2(O1)^p−BD*(O5H6)	0.76	0.067	0.0155
	LP2(O5)−BD*(O8H9)	0.95	0.087	0.0168
	LP2(O8)−BD*(C2H3)	0.84	0.043	0.0052
DW_2	LP1(O1)−BD*(N2H3)	0.96	0.030	0.0024
		1.15	0.043	
	LP3(O1)^p−BD*(N2H3)	0.71	0.066	0.0181
		0.70	0.068	
	LP3(O1)^p−BD*(N2H4)	0.69	0.081	0.0290
		0.68	0.084	
	LP1(O1)−BD*(O5H6)	1.01	0.028	0.0021
		1.19	0.044	
	LP2(O1)−BD*(O5H6)	**1.02**	**0.032**	**0.0010**
	LP3(O1)^p−BD*(O5H6)	0.76	0.082	0.0251
		0.74	0.086	
	LP2(O5)−BD*(O8H9)	0.93	0.095	0.0209
		0.93	0.095	
	LP2(O8)−BD*(N2H3)	0.88	0.091	0.0211
		0.89	0.091	

[a] The p superscript indicates the strong p character of the corresponding orbital. For unrestricted calculations, both α and β contributions are given. The interactions involving the single electron of H_2NO are highlighted in bold.

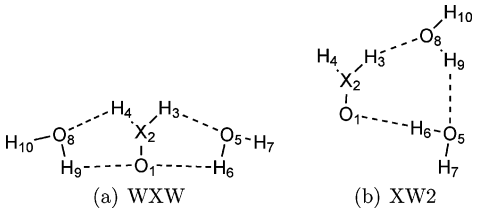

Figure 3. Atom numbering used for the NBO analysis, X = C, N.

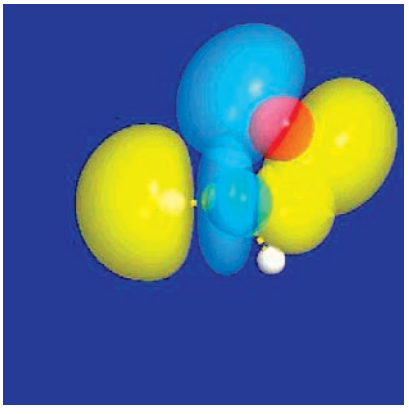

Figure 4. NBO oxygen lone pair interacting with one σ* (N−H) orbital in the dihydronitroxide H_2NO.

orbital in the heterodimers. For the lp (O) → σ* (X−H) intramolecular interaction, the magnitude of the shift Δq_c between the monomers and the dimers supports this interpretation: Δq_c is about 0.9×10^{-2} and 0.6×10^{-2} *e* for the σ* (C−H) orbitals of H_2CO and about 0.6×10^{-2} and 0.4×10^{-2} *e* for the σ* (N−H) orbitals of H_2NO. These values have to be compared to the charge q_c corresponding to lp (O)^p → σ* (O−H) interaction in both heterodimers: about 1.0×10^{-2} *e*.

Moreover, whereas the NBO analysis exhibits a particularly weak interaction between the water oxygen lone pairs and a σ* (C−H) orbital for FW ($q_c = 0.01 \times 10^{-2}$ *e*), a weak but not

negligible interaction between a lone pair of the water oxygen and an antibonding N−H orbital exists in the case of DW: the corresponding charge q_c is 0.4×10^{-2} *e*. Hence, in the case of DW, the incidence of the weakening of the lp $(O)^p \rightarrow \sigma^*$ (N−H) intramolecular interactions is in part counterbalanced by the lp $(O_w) \rightarrow \sigma^*$ (N−H) intermolecular one. As a result, the latter interactions are responsible for a clear decrease in the σ^* (C−H) orbital population for FW, whereas the decrease in the σ^* (N−H) population for DW is much smaller: in terms of q_c, the decrease represents about 16 and 7% of the σ^* (X−H) antibonding populations of the F and D monomers. For the H_2CO systems, this explains the blue shift in the $\bar{\nu}_{C-H}$ frequency observed in FW. Concerning the H_2NO systems, the decrease in the population of the σ^* (N−H) orbital should also lead to a reinforcement of the N−H bond and therefore to a blue shift in the mean $\bar{\nu}_{N-H}$ frequency. This is however not the case, as the latter mean frequency is slightly red-shifted by 9 cm^{-1}.

From the recent discussions of Alabugin and co-workers[11] and of Joseph and Jimmis,[10] we may conclude that when the hyperconjugative interactions lp (Y) $\rightarrow \sigma^*$ (X−H) lead to a weak change in the population of the σ^* (X−H) orbital, the vibrational spectrum of the X−H bond is mainly influenced by higher order electronic density reorganization effects. However, their incidence on this spectrum cannot be readily predicted, especially in the present case where a complex hydrogen bond network is observed in both the FW and the DW dimers.

As the structures of the two WFW and WDW symmetric heterotrimers correspond to those of the FW and DW heterodimers, the same phenomena as above are observed within them, however they are all reinforced (Table 7). For instance, the weakening of the lp $(O)^p \rightarrow \sigma^*$ (X−H) intramolecular hyperconjugation is more pronounced in these trimers: this is echoed in the decrease in the corresponding charges q_c from an average value of 5.1×10^{-2} *e* in FW to an average value of 4.6×10^{-2} *e* in WFW, and from 2.8×10^{-2} to 2.5×10^{-2} *e* in the corresponding nitroxide systems. Concerning WFW, and similarly to FW, the latter intramolecular hyperconjugations are the sole responsible for the occupancy of the σ^* (C−H), and this explains the more accented blue shift in the $\bar{\nu}_{C-H}$ frequency for WFW than for FW (respectively, 78 and 41 cm^{-1}). In the case of WDW, the two symmetric hydrogen bonds between the N−H bonds and the two water oxygens are stronger than the corresponding ones for WFW: they are at the origin of a transfer of 0.44×10^{-2} *e* in the two σ^* (N−H). Hence, for WDW, the intra- and intermolecular hyperconjugative effects counterbalance each other so that the populations of the σ^* (N−H) antibonding orbitals are almost equal in WDW and in DW (respectively, 3.08×10^{-2} and 3.07×10^{-2} *e* on average). Hence, because of the similarities between DW and WDW, we expect a small red shift in the $\bar{\nu}_{N-H}$ frequency for the latter symmetric trimer, which is confirmed by our computations: -17 cm^{-1}.

Last, concerning WFW and WDW, and as expected from their symmetric structures, the total charge q_c "transferred" from the lone pairs of the H_2XO oxygen atom toward the σ^* (O−H) orbitals are equal for the two water molecules. Moreover, these charges are practically the same regardless of the nature of H_2XO: 0.92×10^{-2} *e* and 0.98×10^{-2} *e*, respectively, for WFW and WDW.

As compared to the above symmetric heterotrimers, the NBO results exhibit a different electronic redistribution pattern within the molecules constituting the cyclic trimers (Table 8). First of all, the intermolecular hyperconjugations lp (O) $\rightarrow \sigma^*$ (O−H) are approximately from 2 (1.8×10^{-2} *e* for FW_2) to 3 times (2.8×10^{-2} *e* for DW_2) stronger than in the heterodimers and the symmetric trimers. This is related to the stronger linear character of the $OH_w\cdots O$ hydrogen bonds in the cyclic trimers ($\angle OH_wO > 160°$) than in the remaining oligomers ($\angle OH_wO < 146°$), allowing stronger interactions between the H_2XO oxygen lone pairs and the σ^* (O−H). Concerning the intramolecular lp $(O)^p \rightarrow \sigma^*$ (X−H) interactions, their corresponding charge q_c are smaller than in the symmetric trimers for the X−H bond involved in the hydrogen bond with a water molecule (by 0.7×10^{-2} and 0.6×10^{-2} *e*, respectively, for FW_2 and DW_2), whereas they are practically equal to those of the dimers in the case of the X−H bond not involved in such intermolecular interactions: about 5.2×10^{-2} and 2.9×10^{-2} *e*, respectively, for FW_2 and DW_2.

Last, the main difference between the symmetric trimers (and therefore the dimers) and the cyclic trimers originates from the strength of the hydrogen bonds between the X−H bond of the H_2XO moiety and the second water molecule: they are strongly reinforced in cyclic trimers regardless of the nature of H_2XO (their corresponding q_c values are 0.52×10^{-2} and 2.11×10^{-2} *e*, respectively, for FW_2 and DW_2). These hydrogen bonds have a stronger linear character in the cyclic trimers (their corresponding $\angle XHO_w$ angle values are 146° for FW_2 and 158° for DW_2) than in the dimers and in the symmetric trimers (about 100° for FW and WFW and 120° for DW and WDW), which favors the interactions among the water oxygen lone pairs and the σ^* (X−H) orbitals.

Hence, together, all the above results concerning the hyperconjugative interactions in the cyclic trimers exhibit a large increase in the population of the σ^* (X−H) orbitals as compared to the symmetric trimers. That explains for instance why the mean blue shift in the $\bar{\nu}_{C-H}$ frequency is smaller in FW_2 than in WFW (namely, 54 and 78 cm^{-1}). In the case of DW_2, the latter increase is so large that the population of the σ^* (N−H) orbital corresponding to the bond involved in a hydrogen bond with a water molecule is even larger than in the D isolated monomer. That leads to a red shift in the average $\bar{\nu}_{N-H}$ frequency for DW_2 larger by an order of magnitude than for WDW and DW (namely, -83, -17, and -9 cm^{-1}).

3.3.2. Does the Single Electron Influence the Hydrogen Bond Network of Dihydronitroxide/Water Systems? Reed et al.[8] pointed out the donor capacity of the nitric oxide to form the so-called "half hydrogen bonds" with HF, which can be formed whatever angle HF approaches NO. In analogy with the HF/NO system, the dihydronitroxide may form such a type of hydrogen bond with a water molecule, as long as no other interaction imposes some directionality to the hydrogen bond. However, in the three complexes studied in this work, DW, DW2, and WDW, the water molecules are always involved in two simultaneous hydrogen bonds, restricting strongly the range of the approach angles. Actually, hydrogen bonds are always located in the mean plane of dihydronitroxide. Consequently, the single electron (located in a π^* orbital) cannot directly influence the hydrogen bond network. NBO results support this explanation, since no or very weak intermolecular hyperconjugative interactions are evidenced between this π^* orbital and a water molecule (q_c is at most 0.1×10^{-2} *e*).

Note that Lewis structure-like NBOs assign the NO π electrons to two α-spin lone pairs on N and O and to one β-spin π^* NO orbital, reflecting the three-electron nature of the N−O π bond. Hence, two resonating Lewis structures can be drawn, as reported in Figure 5. Obviously, in the presence of a polar solvent like water, the zwitterionic structure is preferred.

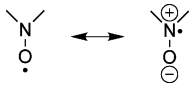

Figure 5. Resonance structures of the nitroxide moiety.

Accordingly, the spin density is mainly located on the nitrogen side, favoring an almost planar structure of the nitroxide moiety.

3.3.3. Hyperconjugation and Cooperative Effects. The strong incidence of cooperative effects upon hydrogen bond networks presenting a cyclic donor/acceptor pattern can be interpreted as originating from a reinforcement of the hyperconjugative interactions within them. The charge transferred q_c from a lone pair of a given molecule toward the σ^* (X−H) antibonding orbital of a second molecule destabilizes the lone pairs of the latter one. As a result, if this molecule is also involved in a new hydrogen bond, this destabilization will reinforce the hyperconjugative interactions between its lone pairs and the σ^* (X−H) orbitals of a third molecule, and so on.

Such a mechanism can be also proposed to explain the strong incidence of cooperative effects on the two FW_2 and DW_2 cyclic trimers: in this particular case, the destabilization of the oxygen lone pairs of the H_2XO moiety is due to the charge-transfer effects occurring between the water oxygen lone pairs and the σ^* (X−H) antibonding orbitals, which destabilize the lp (O) → σ^* (X−H) intramolecular hyperconjugative interaction.

However, intermolecular many-body polarization phenomena have been shown to play also a pivotal role in the interactions among the different monomers of the cyclic oligomers.[35] The dipole moment of the D isolated monomer is larger by 0.7 Debye compared to that of F (3.21 and 2.47 Debye, respectively, at the B3LYP/6-311+G(d,p) level), which suggests that the intermolecular polarization interactions have to be stronger for DW_2 than for FW_2. That may explain the slightly stronger incidence of cooperative effects on DW_2 than on FW_2. Note that the dipole analysis of the NBO Lewis structure allows one to recast the polarization in terms of NBO dipole contributions and hyperconjugative corrections.[8] The X−O oxygen lone pair dipole enhancements due to intra- and intermolecular hyperconjugations are reported in Table 9. It is apparent that the stronger cooperative effects in DW_2 are highlighted by the leading corrective term, arising from the intermolecular lp (O) → σ^* (O−H) hyperconjugation. Contrary to DW_2, the leading corrections to the C−O NBO dipole in FW_2 are due to intramolecular lp (O) → σ^* (C−H) hyperconjugation. The comparison of Tables 8 and 9 clearly shows the same trends. A preferred intramolecular charge transfer in FW_2 leads to a small enhancement of the N−O dipole. However in DW_2, the charge transfers to the N−H and to the water H−O antibonding orbitals are of same magnitude, resulting in a larger intermolecular contribution to the N−O dipole. This result further demonstrates the validity and the consistency of the hyperconjugative picture adopted in this study.

TABLE 9: Hyperconjugation Correction (in Debye) to the X−O NBO Contribution to the Dipole[a]

		$\delta\mu$
F	LP2(O1)^p−BD*(C2H3)	0.48
	LP2(O1)^p−BD*(C2H4)	0.48
FW	LP2(O1)^p−BD*(C2H3)	0.41
	LP2(O1)^p−BD*(C2H4)	0.45
	LP2(O1)^p−BD*(O5H6)	0.20
FW_2	LP2(O1)^p−BD*(C2H3)	0.34
	LP2(O1)^p−BD*(C2H4)	0.44
	LP2(O1)^p−BD*(O5H6)	0.27
D	LP3(O1)^p−BD*(N2H3)	0.14
		0.15
	LP3(O1)^p−BD*(N2H4)	0.14
		0.15
DW	LP3(O1)^p−BD*(N2H3)	0.11
		0.12
	LP3(O1)^p−BD*(N2H4)	0.13
		0.14
	LP3(O1)^p−BD*(O5H6)	0.11
		0.12
DW_2	LP3(O1)^p−BD*(N2H3)	0.08
		0.08
	LP3(O1)^p−BD*(N2H4)	0.13
		0.14
	LP3(O1)^p−BD*(O5H6)	0.20
		0.22

[a] For unrestricted calculations, both α and β contributions are given.

4. Conclusion

In this work, some model nitroxide/water and carbonyl/water clusters have been studied in order to compare their properties, with particular emphasis on the hydrogen bond network.

Our results clearly exhibit that the properties of hydrogen bonds involving a nitroxyl group are very close to those of hydrogen bonds involving a carbonyl group. The main difference between the H_2XO/water aggregates considered in the present paper results principally from the nature of the $XH\cdots O_w$ interaction, which corresponds either to a conventional red-shifting hydrogen bond (within DW, WDW, and DW_2) or to an improper blue-shifting one (within FW_2, FW, and WFW). Last, our results exhibit that almost all the properties of the hydrogen bonds occurring in the model clusters can be interpreted by considering only inter- and intramolecular lp (O) → σ^* (X−H) hyperconjugation arguments.

Our results also suggest that it should be possible to accurately describe the solvation of nitroxide species using atomistic force fields and molecular dynamics techniques, which were shown to provide a reliable description of carbonyl−water hydrogen bonds (cf., for example, ref 36). Such a way of theoretically investigating the properties of solvated nitroxides is presently under investigation in our group, and our first results will be presented soon.

Supporting Information Available: Geometrical, electronic, energetic, and natural bond orbital results at all levels of theory. This material is available free of charge via the Internet at http://pubs.acs.org.

References and Notes

(1) Ottaviani, M. F.; Sacchi, B.; Turro, N. J.; Chen, W.; Jockusch, S.; Tomalia, D. A. *Macromolecules* **1999**, *32*, 2275.

(2) Morin, B.; Bourhis, J.-M.; Belle, V.; Woudstra, M.; Carrière, F.; Guigliarelli, B.; Fournel, A.; Longhi, S. *J. Phys. Chem. B* **2006**, *110*, 20596.

(3) Benoit, D.; Grimaldi, S.; Robin, S.; Finet, J.-P.; Tordo, P.; Gnanou, Y. *J. Am. Chem. Soc.* **2000**, *122*, 5929.

(4) Davies, M. J. Recent Developments in EPR Spin-Trapping. In *Electron Paramagnetic Resonance*; Gilbert, B. C., Davies, M. B., Murphy, D. M., Eds.; The Royal Society of Chemistry: Cambridge, U.K., 2002; Vol. 18, pp 47−73.

(5) Improta, R.; Barone, V. *Chem. Rev.* **2004**, *104*, 1231.

(6) Quack, M.; Suhm, M. In *Conceptual Perspectives in Quantum Chemistry*; Calais, J.-L., Kryachko, E., Eds.; Kluwer Acacdemic Publishers: Dordrecht, The Netherlands, 1997; Vol. III.

(7) Wales, D. In *Encyclopedia of Computational Chemistry*; Schleyer, P. V. R., Ed.; Wiley: Chichester, U.K., 1998; Vol. 5, pp 3183−3193.

(8) Reed, A. E.; Curtiss, L. A.; Weinhold, F. *Chem. Rev.* **1988**, *88*, 899.

(9) Weinhold, F.; Landis, C. Supramolecular Bonding. In *Valency and Bonding: A Natural Bond Orbital Donor-Acceptor Perspective*; Cambridge University Press: Cambridge, U.K., 2005; Chapter 5.

(10) Joseph, J.; Jemmis, E. *J. Am. Chem. Soc.* **2007**, *129*, 4620.

(11) Alabugin, I. V.; Manoharan, M.; Peabody, S.; Weinhold, F. *J. Am. Chem. Soc.* **2003**, *125*, 5973.

(12) Li, A. Y. *J. Chem. Phys.* **2007**, *126*, 154102.
(13) Liu, Y.; Liu, W.; Li, H. J. L.; Yang, Y. *J. Phys. Chem. A* **2006**, *110*, 11760.
(14) Tschumper, G. S.; Leininger, M. L.; Hoffman, B. C.; Valeev, E. F. *J. Chem. Phys.* **2002**, *116*, 690.
(15) Masella, M.; Flament, J.-P. *J. Chem. Phys.* **1999**, *110*, 7245.
(16) Xantheas, S. S.; Burnham, C.; Harrison, R. *J. Chem. Phys.* **2001**, *116*, 1493.
(17) Frisch, M. J.; Trucks, G. W.; Schlegel, H. B.; Scuseria, G. E.; Robb, M. A.; Cheeseman, J. R.; Montgomery, J. A., Jr.; Vreven, T.; Kudin, K. N.; Burant, J. C.; Millam, J. M.; Iyengar, S. S.; Tomasi, J.; Barone, V.; Mennucci, B.; Cossi, M.; Scalmani, G.; Rega, N.; Petersson, G. A.; Nakatsuji, H.; Hada, M.; Ehara, M.; Toyota, K.; Fukuda, R.; Hasegawa, J.; Ishida, M.; Nakajima, T.; Honda, Y.; Kitao, O.; Nakai, H.; Klene, M.; Li, X.; Knox, J. E.; Hratchian, H. P.; Cross, J. B.; Bakken, V.; Adamo, C.; Jaramillo, J.; Gomperts, R.; Stratmann, R. E.; Yazyev, O.; Austin, A. J.; Cammi, R.; Pomelli, C.; Ochterski, J. W.; Ayala, P. Y.; Morokuma, K.; Voth, G. A.; Salvador, P.; Dannenberg, J. J.; Zakrzewski, V. G.; Dapprich, S.; Daniels, A. D.; Strain, M. C.; Farkas, O.; Malick, D. K.; Rabuck, A. D.; Raghavachari, K.; Foresman, J. B.; Ortiz, J. V.; Cui, Q.; Baboul, A. G.; Clifford, S.; Cioslowski, J.; Stefanov, B. B.; Liu, G.; Liashenko, A.; Piskorz, P.; Komaromi, I.; Martin, R. L.; Fox, D. J.; Keith, T.; Al-Laham, M. A.; Peng, C. Y.; Nanayakkara, A.; Challacombe, M.; Gill, P. M. W.; Johnson, B.; Chen, W.; Wong, M. W.; Gonzalez, C.; Pople, J. A. *Gaussian 03*, revision C.02; Gaussian, Inc.: Wallingford, CT, 2004.
(18) Mo, O. M. Y.; Elguero, J. *J. Chem. Phys.* **1992**, *97*, 6628.
(19) Xu, X.; Goddard, W. A. *J. Phys. Chem. A* **2004**, *108*, 2305.
(20) Barone, V.; Bencini, A.; Cossi, M.; Matteo, A. D.; Mattesini, M.; Totti, F. *J. Am. Chem. Soc.* **1998**, *120*, 7069.
(21) Saracino, G. A. A.; Tedeschi, A.; D'Errico, G.; Improta, R.; Franco, L.; Ruzzi, M. C. C.; Barone, V. *J. Phys. Chem. A* **2002**, *106*, 10700.
(22) Villamena, F. A.; Merle, J. K.; Hadad, C. M.; Zweier, J. L. *J. Phys. Chem. A* **2005**, *109*, 6089.
(23) King, B. F.; Weinhold, F. *J. Chem. Phys.* **1995**, *103*, 333.
(24) Xantheas, S. S. *J. Chem. Phys.* **1996**, *104*, 8821.
(25) Simon, S.; Duran, M. *J. Phys. Chem. A* **1999**, *103*, 1640.
(26) Boys, S. F.; Bernardi, F. *Mol. Phys.* **1970**, *19*, 558.
(27) Bader, R. F. W. *Atoms in Molecules: A Quantum Theory*; Oxford University Press Inc.: New York, 1990.
(28) Frisch, M. J.; Trucks, G. W.; Schlegel, H. B.; Scuseria, G. E.; Robb, M. A.; Cheeseman, J. R.; Zakrzewski, V. G.; Montgomery, J. A., Jr.; Stratmann, R. E.; Burant, J. C.; Dapprich, S.; Millam, J. M.; Daniels, A. D.; Kudin, K. N.; Strain, M. C.; Farkas, O.; Tomasi, J.; Barone, V.; Cossi, M.; Cammi, R.; Mennucci, B.; Pomelli, C.; Adamo, C.; Clifford, S.; Ochterski, J.; Petersson, G. A.; Ayala, P. Y.; Cui, Q.; Morokuma, K.; Malick, D. K.; Rabuck, A. D.; Raghavachari, K.; Foresman, J. B.; Cioslowski, J.; Ortiz, J. V.; Stefanov, B. B.; Liu, G.; Liashenko, A.; Piskorz, P.; Komaromi, I.; Gomperts, R.; Martin, R. L.; Fox, D. J.; Keith, T.; Al-Laham, M. A.; Peng, C. Y.; Nanayakkara, A.; Gonzalez, C.; Challacombe, M.; Gill, P. M. W.; Johnson, B. G.; Chen, W.; Wong, M. W.; Andres, J. L.; Head-Gordon, M.; Replogle, E. S.; Pople, J. A. *Gaussian 98*, revision A.9; Gaussian, Inc., Pittsburgh PA, 1998.
(29) Reed, A. E.; Weinstock, R. B.; Weinhold, F. *J. Chem. Phys.* **1985**, *83*, 735.
(30) Barone, V.; Grand, A.; Minichino, C.; Subra, R. *J. Phys. Chem.* **1993**, *97*, 6355.
(31) Barone, V. *Chem. Phys. Lett.* **1996**, *262*, 201.
(32) Simon, S.; Bertran, J.; Sodupe, M. *J. Phys. Chem. A* **2001**, *105*, 4359.
(33) Lee, H.-J.; Choi, Y.-S.; Lee, K.-B.; Park, J.; Yoon, C.-J. *J. Phys. Chem. A* **2002**, *106*, 7010.
(34) Smith, B.; Swanton, D.; Pople, J.; Schaefer, H.; Radom, L. *J. Chem. Phys.* **1990**, *92*, 1240.
(35) Masella, M.; Gresh, N.; Flament, J.-P. *J. Chem. Soc., Faraday Trans.* **1998**, *94*, 2745.
(36) Masella, M.; Cuniasse, P. *J. Chem. Phys.* **2003**, *119*, 1866.